Available online at www.pelagiaresearchlibrary.com

Pelagia Research Library

Advances in Applied Science Research, 2012, 3 (5):3311-3325

ISSN: 0976-8610
CODEN (USA): AASRFC

Oscillatory MHD free convective flow between two vertical walls in a rotating system

Bhaskar Chandra Sarkar[1], Sanatan Das[2] and Rabindra Nath Jana[3]

[1,3]Department of Applied Mathematics, Vidyasagar University, Midnapore 721 102, India
[2]Department of Mathematics, University of Gour Banga , Malda 732 103, India

ABSTRACT

The effects of radiation on oscillatory MHD free convective flow of a viscous incompressible electrically conducting fluid confined between vertical walls in a rotating system have been studied. The flow is due to the periodically oscillating motion of one of the walls. The exact solutions of the governing equations have been obtained by using the Laplace transform technique. The variations of velocity, fluid temperature and shear stress at the moving wall are presented graphically. The velocity components increase with an increase in magnetic parameter. The primary velocity decreases whereas the secondary velocity increases with an increase in radiation parameter. There is an enhancement in fluid temperature as time progresses. The absolute value of the shear stress at the moving wall due to the primary flow increases whereas the absolute value of the shear stress at the moving wall due to the secondary flow decreases with an increase in either rotation parameter or radiation parameter. The rate of heat transfer at the moving wall increases with an increase in radiation parameter.

Keywords: MHD free convection, radiation, rotation, Prandtl number, Grashof number.

INTRODUCTION

Radiative convective flows are encountered in countless industrial and environment processes e.g. heating and cooling chambers, fossil fuel combustion energy processes, evaporation from large open water reservoirs, solar power technology and space vehicle re-entry. Radiative heat transfer plays an important role in manufacturing industries for the design of reliable equipment. Nuclear power plants, gas turbines and various propulsion devices for aircraft, missiles, satellites and space vehicles are examples of such engineering applications. If the temperature of the surrounding fluid is rather high, radiation effects play an important role and this situation does exist in space technology. In such cases, one has to take into account the effect of thermal radiation. The hydrodynamic rotating flow of an electrically conducting viscous incompressible fluids has gained considerable attention because of its numerous applications in physics and engineering. The free convective flow in channels formed by vertical plates has received attention among the researchers in last few decades due to it's widespread importance in engineering applications like cooling of electronic equipments, design of passive solar systems for energy conversion, design of heat exchangers, human comfort in buildings, thermal regulation processes and many more. Many researchers have worked in this field such as Singh [1], Singh et. al. [2], Jha et.al. [3], Joshi [4], Miyatake et. al. [5], Tanaka et. al. [6]. Bestman and Adjepong [7] have studied the unsteady hydromagnetic free- convection flow with radiative heat transfer in a rotating fluid. The transient free convection flow between two vertical parallel plates has been investigated by Singh et al. [8]. Jha [9] has studied the natural Convection in unsteady MHD Couette flow. Narahari et.al.[10] have discussed the transient free convection flow between long vertical parallel plates with constant heat flux at one boundary. The radiation effects on MHD Couette flow with heat transfer between two parallel plates has been examined by Mebine [11]. Jha and Ajibade [12] have studied the unsteady free convective Couette flow of heat generating/absorbing fluid.

The effects of thermal radiation and free convection currents on the unsteady Couette flow between two vertical parallel plates with constant heat flux at one boundary have been studied by Narahari [13]. Kumar and Varma [14] have investigated the radiation effects on MHD flow past an impulsively started exponentially accelerated vertical plate with variable temperature in the presence of heat generation. Rajput and Pradeep [15] have studied the effect of a uniform transverse magnetic field on the unsteady transient free convection flow of an incompressible viscous electrically conducting fluid between two infinite vertical parallel plates with constant temperature and Variable mass diffusion. Rajput and Kumar [16] have discussed the combined effects of rotation and radiation on MHD flow past an impulsively started vertical plate with variable temperature. Reddy et al. [17] have presented the radiation and chemical reaction effects on free convection MHD flow through a porous medium bounded by vertical surface. The unsteady MHD heat and mass transfer free convection flow of polar fluids past a vertical moving porous plate in a porous medium with heat generation and thermal diffusion has been studied by Saxena and Dubey [18]. The mass transfer effects on MHD mixed convective flow from a vertical surface with Ohmic heating and viscous dissipation have been investigated by Babu and Reddy [19]. Saxena and Dubey [20] have analyzed the effects of MHD free convection heat and mass transfer flow of visco-elastic fluid embedded in a porous medium of variable permeability with radiation effect and heat source in slip flow regime. Devi and Gururaj [21] have studied the effects of variable viscosity and nonlinear radiation on MHD flow with heat transfer over a surface stretching with a power-law velocity. The radiation effect on the unsteady MHD convection flow through a non uniform horizontal channel has been studied by Reddy et al. [22]. Das et. al. [23] have investigated the radiation effects on free convection MHD Couette flow started exponentially with variable wall temperature in presence of heat generation. The effect of radiation on transient natural convection flow between two vertical walls has been discussed by Mandal et al.[24]. Das et. al. [25] have studied radiation effects on free convection MHD Couette flow of a viscous incompressible heat generating fluid confined between vertical plates. Recently, Sarkar et. al. [26] have investigated the effects of radiation on MHD free convective couette flow in a rotating system.

In the present paper, our aim is to study the effects of radiation on MHD free convective flow of a viscous incompressible electrically conducting fluid between two infinitely long vertical walls in a rotating system in the presence of an applied transverse magnetic field. It is observed that both the primary velocity u_1 and the secondary velocity v_1 increase with an increase in magnetic parameter M^2. The primary velocity u_1 decreases whereas the secondary velocity v_1 increases with an increase in radiation parameter R. The fluid temperature decreases with an increase in either radiation parameter R or Prandtl number Pr whereas it increases with an increase in time τ. The absolute value of the shear stress τ_{x_0} at the wall $(\eta = 0)$ due to the primary flow increases and the absolute value of the shear stress τ_{y_0} at the wall $(\eta = 0)$ due to the secondary flow decreases with an increase in either radiation parameter R or rotation parameter K^2. Further, the rate of heat transfer $-\theta'(0)$ at the wall $(\eta = 0)$ increases whereas the rate of heat transfer $-\theta'(1)$ at the wall $(\eta = 1)$ decreases with an increase in radiation parameter R.

FORMULATION OF THE PROBLEM AND ITS SOLUTIONS

Consider the unsteady MHD free convective flow of a viscous incompressible electrically conducting fluid between two infinite vertical parallel walls separated by a distance h. Choose a cartesian co-ordinates system with the x - axis along one of the walls in the vertically upward direction and the z - axis normal to the walls and the y -axis is perpendicular to xz -plane [See Fig.1]. The channel and the fluid rotate in unison with a uniform angular velocity Ω about z axis. Initially $(t \le 0)$, both the walls and the fluid are assumed to be at the same temperature T_h and stationary. At time $t > 0$, the wall at $(z = 0)$ suddenly to start move in its own plane with an oscillatory velocity $u_0 \cos \omega^* t$, u_0 being the mean velocity and ω^* being the frequency of the oscillations and it is heated with the temperature $T_h + (T_0 - T_h)\frac{t}{t_0}$, T_0 being the temperature of the wall at $(z = 0)$ and t_0 being constant whereas the wall at $(z = h)$ is stationary and maintained at a constant temperature T_h. A uniform magnetic field of strength B_0 is imposed perpendicular to the walls. It is also assumed that the radiative heat flux in the x -direction is negligible as compared to that in the z - direction. As the walls are infinitely long, the velocity and temperature fields are functions of z and t only.

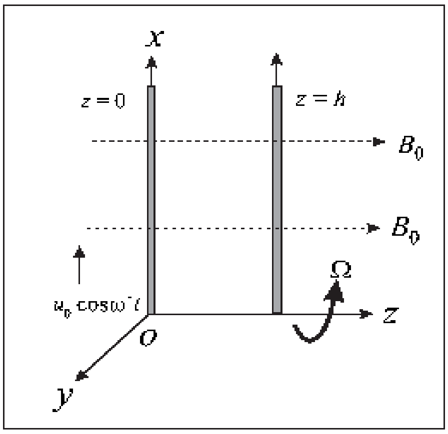

Fig.1: Geometry of the problem

Under the usual Boussinesq's approximation, the fluid flow is governed by the following system of equations

$$\frac{\partial u}{\partial t} - 2\Omega\, v = \nu \frac{\partial^2 u}{\partial z^2} + g\beta^*(T - T_h) - \frac{\sigma B_0^2}{\rho} u, \tag{1}$$

$$\frac{\partial v}{\partial t} + 2\Omega\, u = \nu \frac{\partial^2 v}{\partial z^2} - \frac{\sigma B_0^2}{\rho} v, \tag{2}$$

$$\rho c_p \frac{\partial T}{\partial t} = k \frac{\partial^2 T}{\partial y^2} - \frac{\partial q_r}{\partial z}, \tag{3}$$

where u is the velocity in the x-direction, v is the velocity in the y-direction, g the acceleration due to gravity, T the fluid temperature, β^* the coefficient of thermal expansion, ν the kinematic coefficient of viscosity, ρ the fluid density, σ the electric conductivity, k the thermal conductivity, c_p the specific heat at constant pressure and q_r the radiative heat flux.

The initial and the boundary conditions for velocity and temperature distribution are

$$\begin{aligned} &u = 0 = v,\, T = T_h \quad \text{for} \quad 0 \le z \le h \quad \text{and} \quad t \le 0, \\ &u = u_0 \cos\omega^* t,\; v = 0,\; T = T_h + (T_0 - T_h)\frac{t}{t_0} \quad \text{at} \quad z = 0 \quad \text{for} \quad t > 0, \\ &u = 0 = v,\, T = T_h \quad \text{at} \quad z = h \quad \text{for} \quad t > 0. \end{aligned} \tag{4}$$

It has been shown by Cogley et al.[21] that in the optically thin limit for a non-gray gas near equilibrium, the following relation holds

$$\frac{\partial q_r}{\partial y} = 4(T - T_h)\int_0^\infty K_{\lambda_h^*} \left(\frac{\partial e_{\lambda^* p}}{\partial T}\right)_h d\lambda^*, \tag{5}$$

where K_λ^* is the absorption coefficient, λ^* is the wave length, $e_{\lambda^* p}$ is the Plank's function and subscript $'h'$ indicates that all quantities have been evaluated at the temperature T_h which is the temperature of the plate at time $t \le 0$. Thus, our study is limited to small difference of plate temperature to the fluid temperature.

On the use of the equation (5), equation (3) becomes

$$\rho c_p \frac{\partial T}{\partial t} = k \frac{\partial^2 T}{\partial y^2} - 4(T - T_h) I, \tag{6}$$

where

$$I = \int_0^\infty K_{\lambda_h^*} \left(\frac{\partial e_{\lambda^* p}}{\partial T}\right)_h d\lambda^*. \tag{7}$$

Introducing non-dimensional variables

$$\eta = \frac{z}{h},\;\; \tau = \frac{\nu t}{h^2},\;\; (u_1, v_1) = \frac{(u, v)}{u_0},\; \theta = \frac{T - T_h}{T_0 - T_h}, \tag{8}$$

equations (1), (2) and (6) become

$$\frac{\partial u_1}{\partial \tau} - 2K^2 v_1 = \frac{\partial^2 u_1}{\partial \eta^2} + Gr\theta - M^2 u_1, \tag{9}$$

$$\frac{\partial v_1}{\partial \tau} + 2K^2 u_1 = \frac{\partial^2 v_1}{\partial \eta^2} - M^2 v_1, \tag{10}$$

$$Pr\frac{\partial \theta}{\partial \tau} = \frac{\partial^2 \theta}{\partial \eta^2} - R\theta, \tag{11}$$

where $M^2 = \frac{\sigma B_0^2 h^2}{\rho \nu}$ is the magnetic parameter, $K^2 = \frac{\Omega h^2}{\nu}$ the rotation parameter, $R = \frac{4I h^2}{k}$ the radiation parameter, $Gr = \frac{g\beta^* (T_0 - T_h)h^2}{\nu u_0}$ the Grashof number and $Pr = \frac{\rho \nu c_p}{k}$ the Prandtl number.

The corresponding initial and boundary conditions for u_1 and θ are

$$\begin{aligned} &u_1 = 0 = v_1, \theta = 0 \text{ for } 0 \le \eta \le 1 \text{ and } \tau \le 0, \\ &u_1 = \cos \omega\tau,\ v_1 = 0,\ \theta = \tau \text{ at } \eta = 0 \text{ for } \tau > 0, \\ &u_1 = 0 = v_1,\ \theta = 0 \text{ at } \eta = 1 \text{ for } \tau > 0, \end{aligned} \tag{12}$$

where $\omega = \frac{\omega^* h^2}{\nu}$ is the frequency parameter.

Combining equations (9) and (10), we get

$$\frac{\partial F}{\partial \tau} = \frac{\partial^2 F}{\partial \eta^2} + Gr\theta - \lambda^2 F, \tag{13}$$

where

$$F = u_1 + iv_1,\ \lambda^2 = M^2 + 2iK^2 \text{ and } i = \sqrt{-1}. \tag{14}$$

The initial and the boundary conditions for F and θ are

$$\begin{aligned} &F = 0, \theta = 0 \text{ for } 0 \le \eta \le 1 \text{ and } \tau \le 0, \\ &F = \cos \omega\tau, \theta = \tau \text{ at } \eta = 0 \text{ for } \tau > 0, \\ &F = 0, \theta = 0 \text{ at } \eta = 1 \text{ for } \tau > 0, \end{aligned} \tag{15}$$

Taking Laplace transformation, the equations (13) and (11) become

$$s\bar{F} = \frac{d^2\bar{F}}{d\eta^2} + Gr\bar{\theta} - \lambda^2 \bar{F}, \tag{16}$$

$$Pr\, s\bar{\theta} = \frac{d^2\bar{\theta}}{d\eta^2} - R\bar{\theta}, \tag{17}$$

where

$$\bar{F}(\eta, s) = \int_0^\infty F(\eta, \tau)e^{-s\tau}\, d\tau \text{ and } \bar{\theta}(\eta, s) = \int_0^\infty \theta(\eta, \tau)e^{-s\tau}\, d\tau. \tag{18}$$

The corresponding boundary conditions for $\bar{F}$ and $\bar{\theta}$ are

$$\begin{aligned} &\bar{F}(0, s) = \frac{1}{2}\left(\frac{1}{s - i\omega} + \frac{1}{s + i\omega}\right),\ \bar{\theta}(0, s) = \frac{1}{s^2}, \\ &\bar{F}(1, s) = 0,\ \bar{\theta}(1, s) = 0. \end{aligned} \tag{19}$$

The solution of the equations (16) and (17) subject to the boundary conditions (19) are given by

$$\bar{\theta}(\eta, s) = \begin{cases} \dfrac{1}{s^2}\dfrac{\sinh \sqrt{sPr + R}(1-\eta)}{\sinh \sqrt{sPr + R}} & \text{for } Pr \ne 1 \\ \\ \dfrac{1}{s^2}\dfrac{\sinh \sqrt{s + R}(1-\eta)}{\sinh \sqrt{s + R}} & \text{for } Pr = 1, \end{cases} \tag{20}$$

$$\bar{F}(\eta,s)=\begin{cases}\dfrac{1}{2}\left(\dfrac{1}{s-i\omega}+\dfrac{1}{s+i\omega}\right)\dfrac{\sinh\sqrt{s+\lambda^2}(1-\eta)}{\sinh\sqrt{s+\lambda^2}} \\ +\dfrac{Gr}{(Pr-1)(s+b)s^2}\left[\dfrac{\sinh\sqrt{s+\lambda^2}(1-\eta)}{\sinh\sqrt{s+\lambda^2}}-\dfrac{\sinh\sqrt{sPr+R}(1-\eta)}{\sinh\sqrt{sPr+R}}\right] & \text{for } Pr\neq 1 \\ \dfrac{1}{2}\left(\dfrac{1}{s-i\omega}+\dfrac{1}{s+i\omega}\right)\dfrac{\sinh\sqrt{s+\lambda^2}(1-\eta)}{\sinh\sqrt{s+\lambda^2}} \\ +\dfrac{Gr}{(R-\lambda^2)s^2}\left[\dfrac{\sinh\sqrt{s+\lambda^2}(1-\eta)}{\sinh\sqrt{s+\lambda^2}}-\dfrac{\sinh\sqrt{s+R}(1-\eta)}{\sinh\sqrt{s+R}}\right] & \text{for } Pr=1,\end{cases} \tag{21}$$

where $b=\dfrac{R-\lambda^2}{Pr-1}$.

Then the inverse Laplace transforms of equations (20) and (21) give the solution for the temperature and the velocity distributions as

$$\theta(\eta,\tau)=\begin{cases}\tau\dfrac{\sinh\sqrt{R}(1-\eta)}{\sinh\sqrt{R}}+\dfrac{Pr}{2\sqrt{R}\sinh^2\sqrt{R}}\Big[(1-\eta)\cosh\sqrt{R}(1-\eta)\sinh\sqrt{R} \\ -\sinh\sqrt{R}(1-\eta)\cosh\sqrt{R}\Big]+2\displaystyle\sum_{n=1}^{\infty}n\pi\dfrac{e^{s_1\tau}}{s_1^2 Pr}\sin n\pi\eta & \text{for } Pr\neq 1 \\ \tau\dfrac{\sinh\sqrt{R}(1-\eta)}{\sinh\sqrt{R}}+\dfrac{1}{2\sqrt{R}\sinh^2\sqrt{R}}\Big[(1-\eta)\cosh\sqrt{R}(1-\eta)\sinh\sqrt{R} \\ -\sinh\sqrt{R}(1-\eta)\cosh\sqrt{R}\Big]+2\displaystyle\sum_{n=1}^{\infty}n\pi\dfrac{e^{s_1\tau}}{s_1^2}\sin n\pi\eta & \text{for } Pr=1,\end{cases} \tag{22}$$

$$F(\eta,\tau)=\begin{cases}\dfrac{1}{2}\left[e^{i\omega\tau}\dfrac{\sinh\sqrt{\lambda^2+i\omega}(1-\eta)}{\sinh\sqrt{\lambda^2+i\omega}}+e^{-i\omega\tau}\dfrac{\sinh\sqrt{\lambda^2-i\omega}(1-\eta)}{\sinh\sqrt{\lambda^2-i\omega}}\right] \\ +\displaystyle\sum_{n=1}^{\infty}n\pi e^{s_2\tau}\left[\dfrac{1}{s_2-i\omega}+\dfrac{1}{s_2+i\omega}\right]\sin n\pi\eta+F_1(\eta,\tau,\lambda,Pr,\sqrt{R}) & \text{for } Pr\neq 1 \\ \dfrac{1}{2}\left[e^{i\omega\tau}\dfrac{\sinh\sqrt{\lambda^2+i\omega}(1-\eta)}{\sinh\sqrt{\lambda^2+i\omega}}+e^{-i\omega\tau}\dfrac{\sinh\sqrt{\lambda^2-i\omega}(1-\eta)}{\sinh\sqrt{\lambda^2-i\omega}}\right] \\ +\displaystyle\sum_{n=1}^{\infty}n\pi e^{s_2\tau}\left[\dfrac{1}{s_2-i\omega}+\dfrac{1}{s_2+i\omega}\right]\sin n\pi\eta+F_2(\eta,\tau,\lambda,\sqrt{R}) & \text{for } Pr=1,\end{cases} \tag{23}$$

where

$$\begin{aligned}F_1(\eta,\tau,\lambda,Pr,\sqrt{R})=\frac{Gr}{Pr-1}\Bigg[&\frac{1}{b^2}(\tau b-1)\left\{\frac{\sinh\lambda(1-\eta)}{\sinh\lambda}-\frac{\sinh\sqrt{R}(1-\eta)}{\sinh\sqrt{R}}\right\} \\ &+\frac{1}{2b\lambda\sinh^2\lambda}\{(1-\eta)\cosh\lambda(1-\eta)\sinh\lambda-\sinh\lambda(1-\eta)\cosh\lambda\} \\ &-\frac{Pr}{2b\sqrt{R}\sinh^2\sqrt{R}}\{(1-\eta)\cosh\sqrt{R}(1-\eta)\sinh\sqrt{R}-\sinh\sqrt{R}(1-\eta)\cosh\sqrt{R}\} \\ &+2\sum_{n=1}^{\infty}n\pi\left\{\frac{e^{s_2\tau}}{s_2^2(s_2+b)}-\frac{e^{s_1\tau}}{s_1^2(s_1+b)Pr}\right\}\sin n\pi\eta\Bigg],\end{aligned}$$

$$F_2(\eta,\tau,\lambda,\sqrt{R})=\frac{Gr}{R-\lambda^2}\left[\tau\left\{\frac{\sinh\lambda(1-\eta)}{\sinh\lambda}-\frac{\sinh\sqrt{R}(1-\eta)}{\sinh\sqrt{R}}\right\}\right. \tag{24}$$

$$+\frac{1}{2\lambda\sinh^2\lambda}\{(1-\eta)\cosh\lambda(1-\eta)\sinh\lambda-\sinh\lambda(1-\eta)\cosh\lambda\}$$
$$-\frac{1}{2\sqrt{R}\sinh^2\sqrt{R}}\{(1-\eta)\cosh\sqrt{R}(1-\eta)\sinh\sqrt{R}-\sinh\sqrt{R}(1-\eta)\cosh\sqrt{R}\}$$
$$\left.+2\sum_{n=1}^{\infty}n\pi\left\{\frac{e^{s_2\tau}}{s_2{}^2}-\frac{e^{s_1\tau}}{s_1{}^2}\right\}\sin n\pi\eta\right],$$
$$s_1=-\frac{(n^2\pi^2+R)}{Pr},\quad s_2=-(n^2\pi^2+\lambda^2),$$

λ is given by (14). On separating into a real and imaginary parts one can easily obtain the velocity components u_1 and v_1 from equation (23). If the frequency parameter $\omega=0$ then the equation (23) is identical with the equation (23) of Sarkar et. al. [20]. This means in the absence of frequency of oscillations we can obtain the fluid velocity components when the wall at $(\eta=0)$ starts impulsively.

For large time τ, equations (22) and (23) become

$$\theta(\eta,\tau)=\begin{cases}\tau\dfrac{\sinh\sqrt{R}(1-\eta)}{\sinh\sqrt{R}}+\dfrac{Pr}{2\sqrt{R}\sinh^2\sqrt{R}}\Big[(1-\eta)\cosh\sqrt{R}(1-\eta)\sinh\sqrt{R} \\ -\sinh\sqrt{R}(1-\eta)\cosh\sqrt{R}\Big] & \text{for } Pr\neq 1 \\ \tau\dfrac{\sinh\sqrt{R}(1-\eta)}{\sinh\sqrt{R}}+\dfrac{1}{2\sqrt{R}\sinh^2\sqrt{R}}\Big[(1-\eta)\cosh\sqrt{R}(1-\eta)\sinh\sqrt{R} \\ -\sinh\sqrt{R}(1-\eta)\cosh\sqrt{R}\Big] & \text{for } Pr=1,\end{cases}\tag{25}$$

$$F(\eta,\tau)=\begin{cases}\dfrac{1}{2}\left[e^{i\omega\tau}\dfrac{\sinh\sqrt{\lambda^2+i\omega}(1-\eta)}{\sinh\sqrt{\lambda^2+i\omega}}+e^{-i\omega\tau}\dfrac{\sinh\sqrt{\lambda^2-i\omega}(1-\eta)}{\sinh\sqrt{\lambda^2-i\omega}}\right] \\ +F_1(\eta,\tau,\lambda,Pr,\sqrt{R}) & \text{for } Pr\neq 1 \\ \dfrac{1}{2}\left[e^{i\omega\tau}\dfrac{\sinh\sqrt{\lambda^2+i\omega}(1-\eta)}{\sinh\sqrt{\lambda^2+i\omega}}+e^{-i\omega\tau}\dfrac{\sinh\sqrt{\lambda^2-i\omega}(1-\eta)}{\sinh\sqrt{\lambda^2-i\omega}}\right] \\ +F_2(\eta,\tau,\lambda,\sqrt{R}) & \text{for } Pr=1,\end{cases}\tag{26}$$

where

$$F_1(\eta,\tau,\lambda,Pr,\sqrt{R})=\frac{Gr}{Pr-1}\left[\frac{1}{b^2}(\tau b-1)\left\{\frac{\sinh\lambda(1-\eta)}{\sinh\lambda}-\frac{\sinh\sqrt{R}(1-\eta)}{\sinh\sqrt{R}}\right\}\right.$$
$$+\frac{1}{2b\lambda\sinh^2\lambda}\{(1-\eta)\cosh\lambda(1-\eta)\sinh\lambda-\sinh\lambda(1-\eta)\cosh\lambda\}$$
$$\left.-\frac{Pr}{2b\sqrt{R}\sinh^2\sqrt{R}}\{(1-\eta)\cosh\sqrt{R}(1-\eta)\sinh\sqrt{R}-\sinh\sqrt{R}(1-\eta)\cosh\sqrt{R}\}\right],$$

$$F_2(\eta,\tau,\lambda,\sqrt{R})=\frac{Gr}{R-\lambda^2}\left[\tau\left\{\frac{\sinh\lambda(1-\eta)}{\sinh\lambda}-\frac{\sinh\sqrt{R}(1-\eta)}{\sinh\sqrt{R}}\right\}\right.\tag{27}$$
$$+\frac{1}{2\lambda\sinh^2\lambda}\{(1-\eta)\cosh\lambda(1-\eta)\sinh\lambda-\sinh\lambda(1-\eta)\cosh\lambda\}$$
$$\left.-\frac{1}{2\sqrt{R}\sinh^2\sqrt{R}}\{(1-\eta)\cosh\sqrt{R}(1-\eta)\sinh\sqrt{R}-\sinh\sqrt{R}(1-\eta)\cosh\sqrt{R}\}\right]$$

and λ is given by (14).

RESULTS AND DISCUSSION

We have presented the non-dimensional velocity and temperature distributions for several values of magnetic parameter M^2, rotation parameter K^2, Grashof number Gr, radiation parameter R, Prandtl number Pr, time τ and frequency parameter ω in Figs.2-11. It is seen from Fig.2 that the primary velocity u_1 and the secondary velocity v_1 increase with an increase in magnetic parameter M^2. This indicates that the applied magnetic field is effectively moving with the free stream. The resulting Lorenzian body force will therefore not act as a drag force as in conventional MHD flows, but as an aiding body force. This will serve to accelerate the fluid velocity components. Fig.3 reveals that the primary velocity u_1 decreases in the region $0 \le \eta < 0.46$ and it vanishes at a critical distance from the wall which is approximately at $(\eta = 0.46)$ and then it increases whereas the secondary velocity v_1 increases in the region $0 \le \eta < 0.14$ and it vanishes at a critical distance from the wall which is approximately at $(\eta = 0.14)$ and then it decreases with an increase in rotation parameter K^2. The rotation parameter K^2 defines the relative magnitude of the Coriolis force and the viscous force in the regime, therefore it is clear that the high magnitude Coriolis forces are counter-productive for the primary velocity. It is observed from Fig.4 that the primary velocity u_1 increases whereas the secondary velocity v_1 decreases with an increase in Grashof number Gr. It means that the buoyancy force has an accelerating influence on primary velocity while it has a retarding influence on secondary velocity. Back flow arises in the second half of the channel as buoyancy force increases. For $R < 1$, thermal conduction exceeds thermal radiation and for $R > 1$ this situation is reversed. For $R = 1$, the contribution from both modes is equal. It is seen from Fig.5 that an increase in radiation parameter R leads to a decrease in the primary velocity u_1 and increase in secondary velocity v_1. Back flow arises in the second half of the channel with an increase in radiation parameter. Fig.6 shows that the the primary velocity u_1 decreases whereas the secondary velocity v_1 increases near the wall $(\eta = 0)$ and it decreases away from the wall $(\eta = 0)$ with an increase in Prandtl number Pr. Physically, this is true because the increase in the Prandtl number is due to increase in the viscosity of the fluid which makes the fluid thick and hence causes a decrease in the primary velocity of the fluid. It is revealed from Fig.7 that the primary velocity u_1 decreases in the region $0 \le \eta < 0.32$ and then increases whereas secondary velocity v_1 decreases with an increase in time τ. It is seen from Fig.8 that both the primary velocity u_1 and the secondary velocity v_1 decrease near the wall $(\eta = 0)$ and increase away from the wall $(\eta = 0)$ with an increase in frequency parameter ω. The critical distances from the wall $(\eta = 0)$ of the primary and the secondary velocity are approximately at $(\eta = 0.34)$ and $(\eta = 0.52)$ respectively. Further, it is seen from Figs.3-8 that the value of the fluid velocity components become negative at some region between two walls which indicates that there occurs a reverse flow at that region. Physically this is possible as the motion of the fluid is due to the wall motion in the upward direction against the gravitational field.

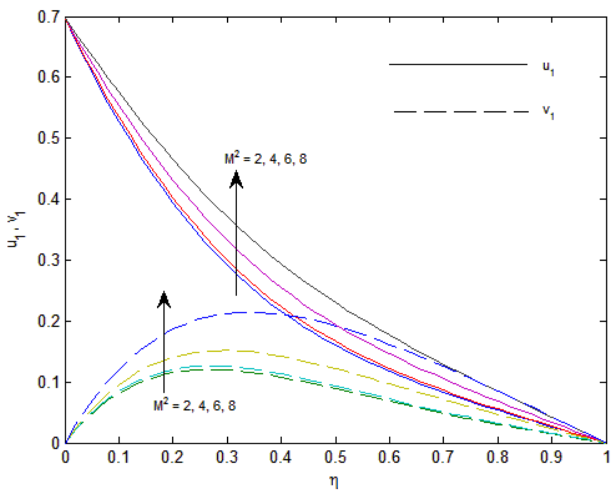

Fig.2: Velocity components for M^2 **when** $R=1$, $K^2=5$, $Pr=0.03$, $Gr=5$, $\omega=4$ **and** $\tau=0.2$

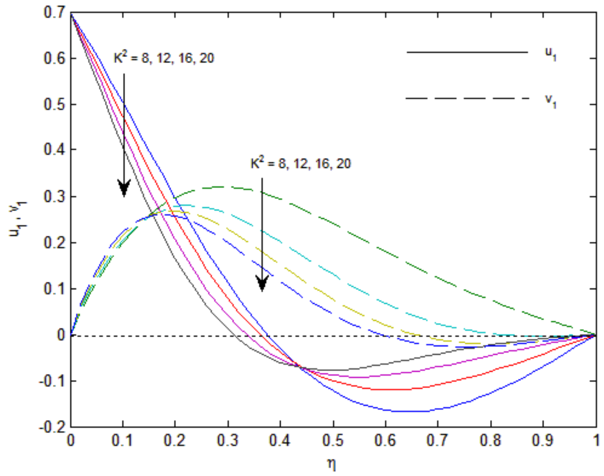

Fig.3: Velocity components for K^2 **when** $R=1$, $M^2=15$, $Pr=0.03$, $Gr=5$, $\omega=4$ **and** $\tau=0.2$

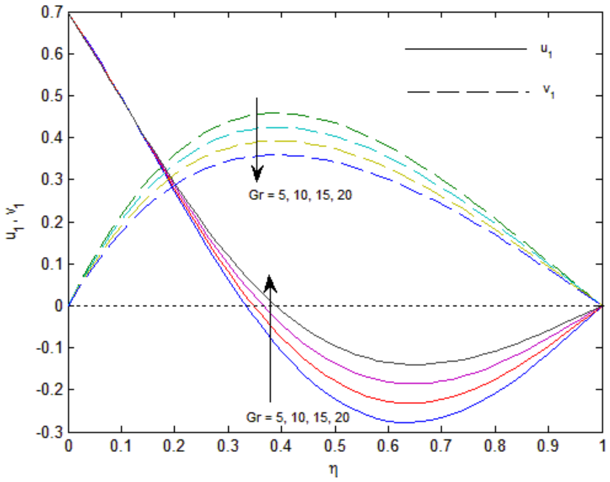

Fig.4: Velocity components for Gr **when** $R=1$, $M^2=15$, $Pr=0.03$, $K^2=5$, $\omega=4$ **and** $\tau=0.2$

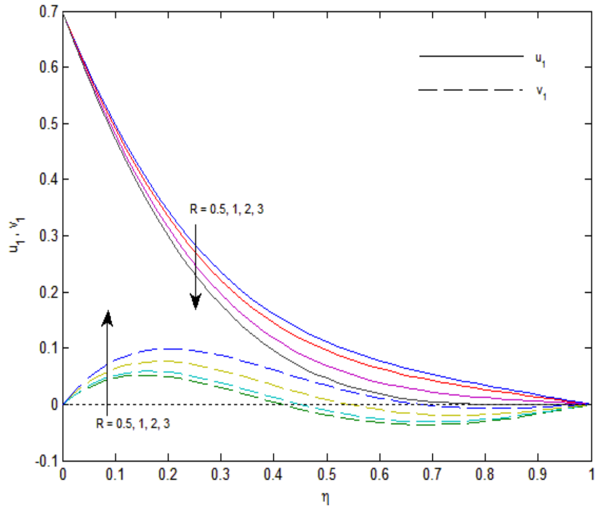

Fig.5: Velocity components for R **when** $Gr=15$, $M^2=2$, $Pr=0.03$, $K^2=5$, $\omega=4$ **and** $\tau=0.2$

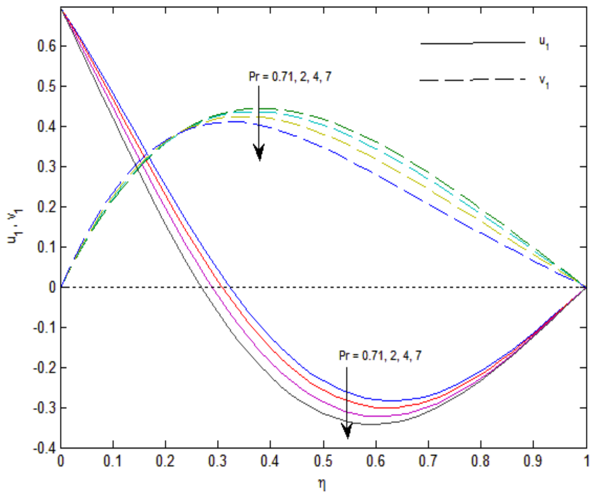

Fig.6: Velocity components for Pr **when** $R=5$, $M^2=15$, $Gr=5$, $K^2=5$, $\omega=4$ **and** $\tau=0.2$

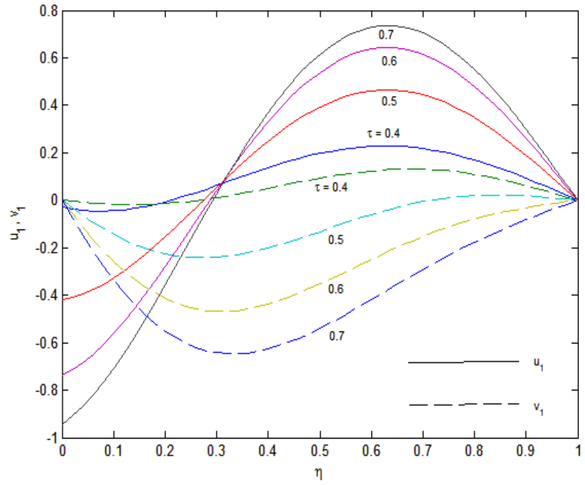

Fig.7: Velocity components for τ **when** $R=1$, $M^2=15$, $Gr=5$, $K^2=5$, $\omega=4$ **and** $Pr=0.03$

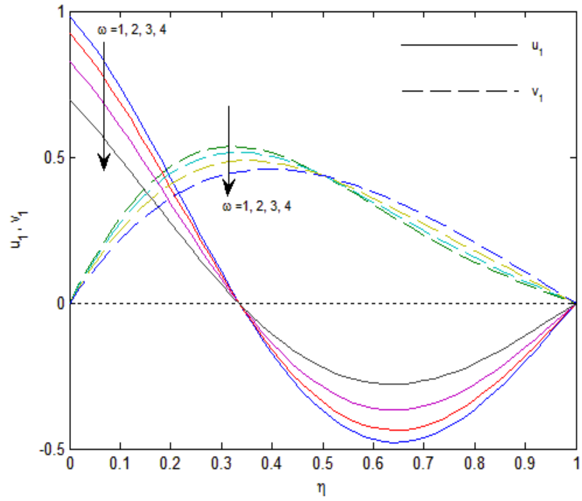

Fig.8: Velocity components for ω **when** $M^2=15$, $R=1$, $K^2=5$, $Pr=0.03$, $Gr=5$ **and** $\tau=0.2$

The effects of radiation parameter R, Prandtl number Pr and time τ on the temperature distribution have been shown in Figs.9-11. It is observed from Fig.9 that the fluid temperature θ decreases with an increase in radiation parameter R. This result qualitatively agrees with expectations, since the effect of radiation decrease the rate of energy transport to the fluid, thereby decreasing the temperature of the fluid. Fig.10 shows that the fluid temperature θ decreases with an increase in Prandtl number Pr. Prandtl number Pr is the ratio of viscosity to thermal diffusivity. An increase in thermal diffusivity leads to a decrease in Prandtl number. Therefore, thermal diffusion has tendency to reduce the fluid temperature. It is revealed from Fig.11 that an increase in time τ leads to rise in the fluid temperature distribution θ. It indicates that there is an enhancement in fluid temperature as time progresses.

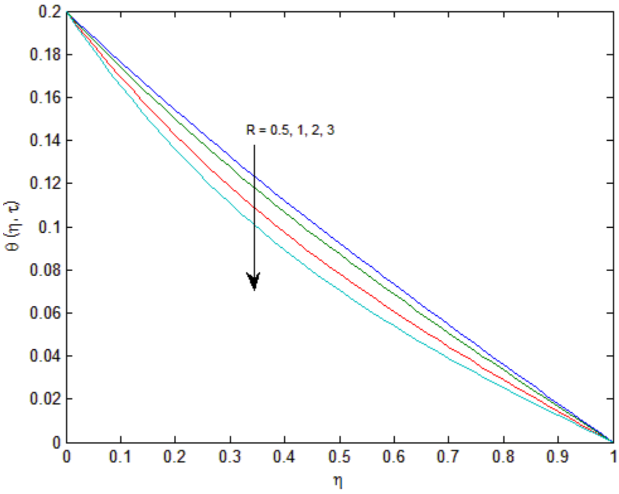

Fig.9: Temperature profiles for R **when** $\tau = 0.2$ **and** $Pr = 0.03$

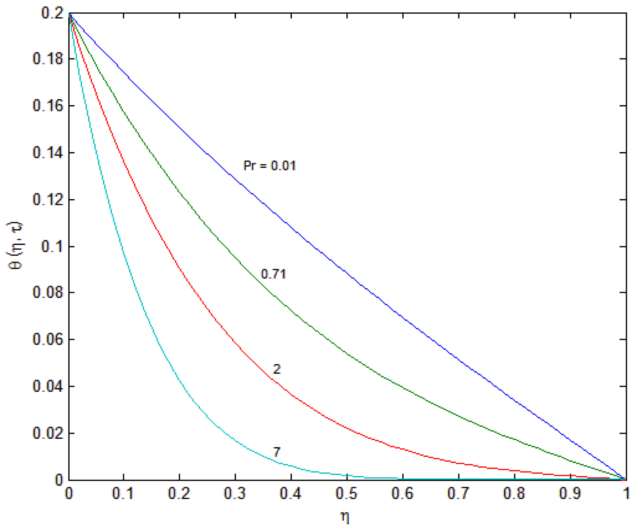

Fig.10: Temperature profiles for Pr **when** $\tau = 0.2$ **and** $R = 1$

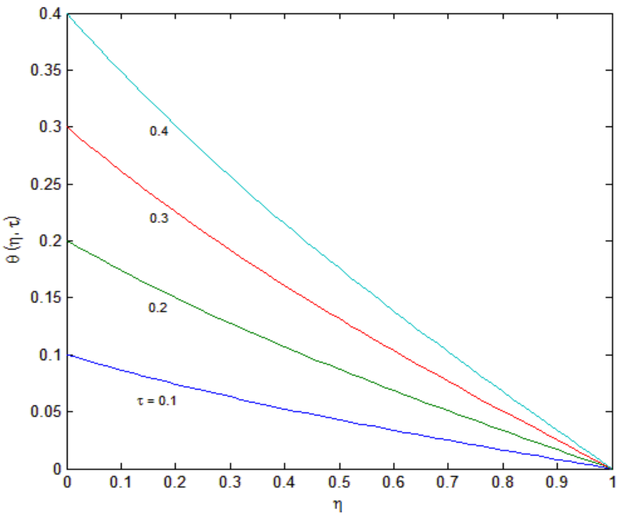

Fig.11: Temperature profiles for τ **when** $R = 1$ **and** $Pr = 0.03$

The non-dimensional shear stress at the wall $(\eta = 0)$ and at the wall $(\eta = 1)$ are respectively obtained as follows:

$$\tau_{x_0}+i\tau_{y_0}=\left(\frac{\partial F}{\partial\eta}\right)_{\eta=0}$$

$$=\begin{cases}-\frac{1}{2}\left[\sqrt{\lambda^2+i\omega}\,e^{i\omega\tau}\coth\sqrt{\lambda^2+i\omega}+\sqrt{\lambda^2-i\omega}\,e^{-i\omega\tau}\coth\sqrt{\lambda^2-i\omega}\right] & \\ +\sum_{n=1}^{\infty}n^2\pi^2e^{s_2\tau}\left[\frac{1}{s_2-i\omega}+\frac{1}{s_2+i\omega}\right]+G_1(0,\tau,\lambda,Pr,\sqrt{R}) & \text{for } Pr\neq 1 \\ -\frac{1}{2}\left[\sqrt{\lambda^2+i\omega}\,e^{i\omega\tau}\coth\sqrt{\lambda^2+i\omega}+\sqrt{\lambda^2-i\omega}\,e^{-i\omega\tau}\coth\sqrt{\lambda^2-i\omega}\right] & \\ +2\sum_{n=1}^{\infty}n^2\pi^2e^{s_2\tau}\left[\frac{1}{s_2-i\omega}+\frac{1}{s_2+i\omega}\right]+G_2(0,\tau,\lambda,\sqrt{R}) & \text{for } Pr=1,\end{cases}\tag{28}$$

$$\tau_{x_1}+i\tau_{y_1}=\left(\frac{\partial F}{\partial\eta}\right)_{\eta=1}$$

$$=\begin{cases}-\frac{1}{2}\left[\sqrt{\lambda^2+i\omega}\,e^{i\omega\tau}\operatorname{cosech}\sqrt{\lambda^2+i\omega}+\sqrt{\lambda^2-i\omega}\,e^{-i\omega\tau}\operatorname{cosech}\sqrt{\lambda^2-i\omega}\right] & \\ +\sum_{n=1}^{\infty}n^2\pi^2(-1)^ne^{s_2\tau}\left[\frac{1}{s_2-i\omega}+\frac{1}{s_2+i\omega}\right]+G_1(1,\tau,\lambda,Pr,\sqrt{R}) & \text{for } Pr\neq 1 \\ -\frac{1}{2}\left[\sqrt{\lambda^2+i\omega}\,e^{i\omega\tau}\operatorname{cosech}\sqrt{\lambda^2+i\omega}+\sqrt{\lambda^2-i\omega}\,e^{-i\omega\tau}\operatorname{cosech}\sqrt{\lambda^2-i\omega}\right] & \\ +\sum_{n=1}^{\infty}n^2\pi^2(-1)^ne^{s_2\tau}\left[\frac{1}{s_2-i\omega}+\frac{1}{s_2+i\omega}\right]+G_2(1,\tau,\lambda,\sqrt{R}) & \text{for } Pr=1,\end{cases}\tag{29}$$

where

$$\begin{aligned}G_1(0,\tau,\lambda,Pr,\sqrt{R})&=\frac{Gr}{Pr-1}\left[\frac{1}{b^2}(\tau b-1)\left(\sqrt{R}\coth\sqrt{R}-\lambda\coth\lambda\right)+\frac{1}{2b\lambda\sinh^2\lambda}(\lambda-\cosh\lambda\sinh\lambda)\right.\\&\left.-\frac{Pr}{2b\sqrt{R}\sinh^2\sqrt{R}}\left(\sqrt{R}-\cosh\sqrt{R}\sinh\sqrt{R}\right)+2\sum_{n=1}^{\infty}n^2\pi^2\left\{\frac{e^{s_2\tau}}{s_2^{\,2}(s_2+b)}-\frac{e^{s_1\tau}}{s_1^{\,2}(s_1+b)Pr}\right\}\right],\\G_1(1,\tau,\lambda,Pr,\sqrt{R})&=\frac{Gr}{Pr-1}\left[\frac{1}{b^2}(\tau b-1)\left(\sqrt{R}\operatorname{cosech}\sqrt{R}-\lambda\operatorname{cosech}\lambda\right)+\frac{1}{2b\lambda\sinh^2\lambda}(\lambda\cosh\lambda-\sinh\lambda)\right.\\&-\frac{Pr}{2b\sqrt{R}\sinh^2\sqrt{R}}\left(\sqrt{R}\cosh\sqrt{R}-\sinh\sqrt{R}\right)\\&\left.+2\sum_{n=1}^{\infty}n^2\pi^2(-1)^n\left\{\frac{e^{s_2\tau}}{s_2^{\,2}(s_2+b)}-\frac{e^{s_1\tau}}{s_1^{\,2}(s_1+b)Pr}\right\}\right],\\G_2(0,\tau,\lambda,\sqrt{R})&=\frac{Gr}{R-\lambda^2}\left[\tau\left(\sqrt{R}\coth\sqrt{R}-\lambda\coth\lambda\right)+\frac{1}{2\lambda\sinh^2\lambda}(\lambda-\cosh\lambda\sinh\lambda)\right.\\&\left.-\frac{1}{2\sqrt{R}\sinh^2\sqrt{R}}\left(\sqrt{R}-\cosh\sqrt{R}\sinh\sqrt{R}\right)+2\sum_{n=1}^{\infty}n^2\pi^2\left\{\frac{e^{s_2\tau}}{s_2^{\,2}}-\frac{e^{s_1\tau}}{s_1^{\,2}}\right\}\right],\\G_2(1,\tau,\lambda,\sqrt{R})&=\frac{Gr}{R-\lambda^2}\left[\tau\left(\sqrt{R}\operatorname{cosech}\sqrt{R}-\lambda\operatorname{cosech}\lambda\right)+\frac{1}{2\lambda\sinh^2\lambda}(\lambda\cosh\lambda-\sinh\lambda)\right.\\&\left.-\frac{1}{2\sqrt{R}\sinh^2\sqrt{R}}\left(\sqrt{R}\cosh\sqrt{R}-\sinh\sqrt{R}\right)+2\sum_{n=1}^{\infty}n^2\pi^2(-1)^n\left\{\frac{e^{s_2\tau}}{s_2^{\,2}}-\frac{e^{s_1\tau}}{s_1^{\,2}}\right\}\right],\end{aligned}\tag{30}$$

λ is given by (14), s_1 and s_2 are given by (24).

Numerical results of the non-dimensional shear stresses at the wall $(\eta=0)$ are presented in Figs.12-15 against magnetic parameter M^2 for several values of rotation parameter K^2, radiation parameter R, Grashof number Gr and time τ when $Pr = 0.03$. Figs.12 and 13 show that the absolute value of the shear stress τ_{x_0} due to the primary flow at the wall $(\eta = 0)$ increases whereas the absolute value of the shear stress τ_{y_0} due to the secondary flow at the wall $(\eta = 0)$ decreases with an increase in either rotation parameter K^2 or radiation parameter R. It is observed from Fig.14 that the absolute value of the shear stress τ_{x_0} at the wall $(\eta = 0)$ as well as the absolute value of the shear stress τ_{y_0} at the wall $(\eta = 0)$ increase with an increase in Grashof number Gr. It is revealed from Fig.15 that the absolute value of the shear stress τ_{x_0} at the wall $(\eta = 0)$ decreases whereas the absolute value of the shear stress τ_{y_0} at the wall $(\eta = 0)$ increases with an increase in frequency parameter ω. Further, it seen from Figs.12-15 that the absolute value of the shear stress τ_{x_0} due to the primary flow at the wall $(\eta = 0)$ increases with an increase in magnetic parameter M^2. Since the applied magnetic field is translating with the free stream, it induces an acceleration effect in the velocity. Velocities are increased and the shear stress at the wall will therefore be enhanced with an increase in M^2.

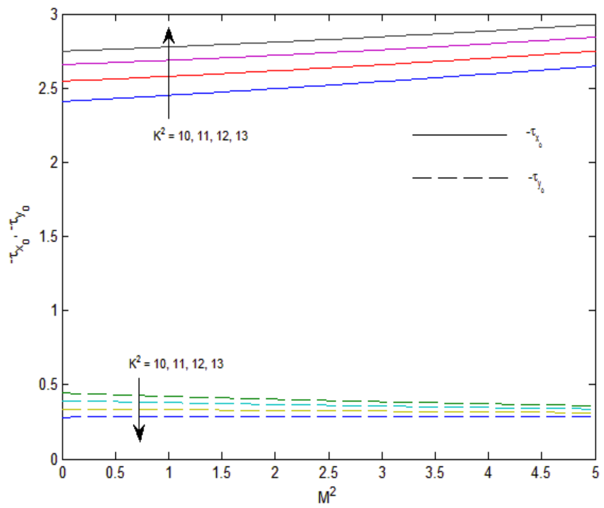

Fig.12: Shear stresses τ_{x_0} **and** τ_{y_0} **for** K^2 **when** $\tau = 0.2$, $R = 1$, $Gr = 5$ **and** $\omega = 4$

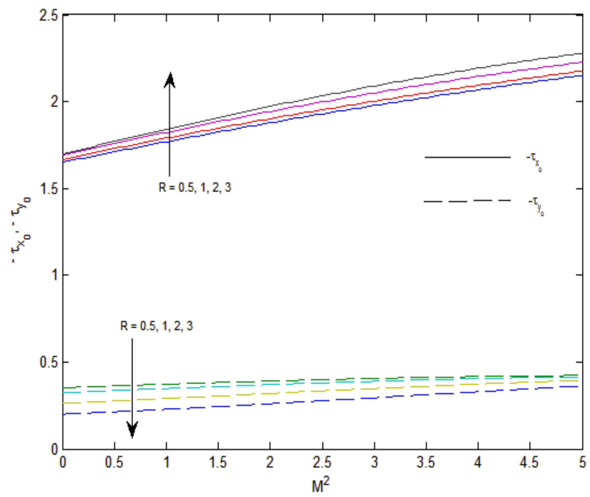

Fig.13: Shear stresses τ_{x_0} **and** τ_{y_0} **for** R **when** $\tau = 0.2$, $K^2 = 5$, $Gr = 5$ **and** $\omega = 4$

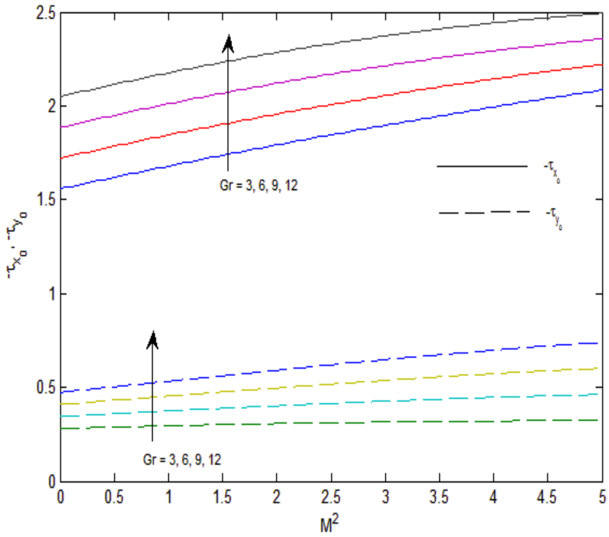

Fig.14: Shear stresses τ_{x_0} **and** τ_{y_0} **for** Gr **when** $\tau = 0.2$, $R = 1$, $K^2 = 5$ **and** $\omega = 4$

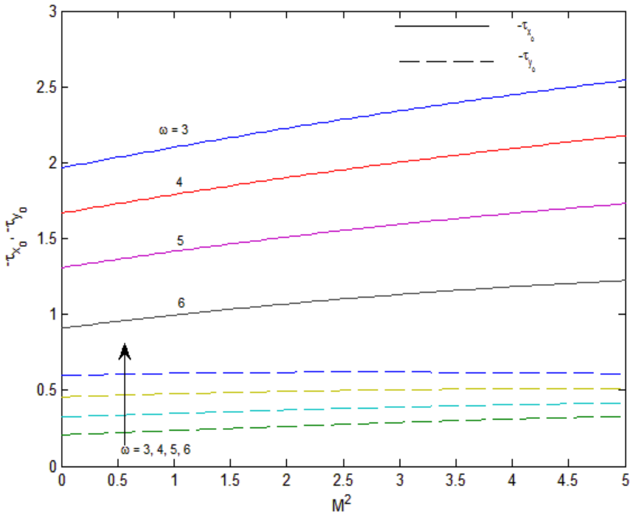

Fig.15: Shear stresses τ_{x_0} **and** τ_{y_0} **for** ω **when** $\tau = 0.2$, $R = 1$, $Gr = 5$ **and** $K^2 = 5$

The rate of heat transfer at the walls $(\eta = 0)$ and $(\eta = 1)$ are obtained as

$$\theta'(0) = \left.\frac{\partial \theta}{\partial \eta}\right|_{\eta=0} = \begin{cases} -\tau\sqrt{R}\coth\sqrt{R} + \dfrac{Pr}{2\sqrt{R}\sinh^2\sqrt{R}}\left[\sqrt{R} - \cosh\sqrt{R}\sinh\sqrt{R}\right] \\ +2\displaystyle\sum_{n=1}^{\infty} n^2\pi^2 \frac{e^{s_1\tau}}{s_1^{\,2}\,Pr} & \text{for } Pr \neq 1 \\ -\tau\sqrt{R}\coth\sqrt{R} + \dfrac{1}{2\sqrt{R}\sinh^2\sqrt{R}}\left[\sqrt{R} - \cosh\sqrt{R}\sinh\sqrt{R}\right] \\ +2\displaystyle\sum_{n=1}^{\infty} n^2\pi^2 \frac{e^{s_1\tau}}{s_1^{\,2}} & \text{for } Pr = 1, \end{cases} \tag{31}$$

$$\theta'(1)=\left.\frac{\partial\theta}{\partial\eta}\right|_{\eta=1}=\begin{cases}-\tau\sqrt{R}\,\mathrm{cosech}\sqrt{R}+\dfrac{Pr}{2\sqrt{R}\sinh^2\sqrt{R}}\left[\sqrt{R}\cosh\sqrt{R}-\sinh\sqrt{R}\right] & \\ +2\displaystyle\sum_{n=1}^{\infty}n^2\pi^2(-1)^n\frac{e^{s_1\tau}}{s_1^2 Pr} & \text{for } Pr\neq 1 \\ -\tau\sqrt{R}\,\mathrm{cosech}\sqrt{R}+\dfrac{1}{2\sqrt{R}\sinh^2\sqrt{R}}\left[\sqrt{R}\cosh\sqrt{R}-\sinh\sqrt{R}\right] & \\ +2\displaystyle\sum_{n=1}^{\infty}n^2\pi^2(-1)^n\frac{e^{s_1\tau}}{s_1^2} & \text{for } Pr=1,\end{cases}\qquad(32)$$

where s_1 is given by (24).

Numerical results of the rate of heat transfer $-\theta'(0)$ at the wall $(\eta=0)$ and the rate of heat transfer $-\theta'(1)$ at the wall $(\eta=1)$ against the radiation parameter R are presented in the Table 1 and 2 for several values of Prandtl number Pr and time τ. Table 1 shows that the rate of heat transfer $-\theta'(0)$ increases whereas $-\theta'(1)$ decreases with an increase in Prandtl number Pr. It is observed from Table 2 that the rate of heat transfer $-\theta'(0)$ as well as $-\theta'(1)$ increase with an increase in time τ. Further, it is seen from Table 1 and 2 that the rate of heat transfer $-\theta'(0)$ increases whereas $-\theta'(1)$ decreases with an increase in radiation parameter R.

Table 1. Rate of heat transfer at the plate $(\eta=0)$ and at the plate $(\eta=1)$

	$-\theta'(0)$				$-\theta'(1)$			
$R\backslash Pr$	0.01	0.71	1	2	0.01	0.71	1	2
0.5	0.23540	0.44719	0.52178	0.72549	0.18277	0.08573	0.05865	0.01529
1.0	0.26555	0.46614	0.53808	0.73721	0.16885	0.08117	0.05599	0.01483
1.5	0.29403	0.48461	0.55407	0.74881	0.15635	0.07690	0.05346	0.01438
2.0	0.32102	0.50262	0.56976	0.76030	0.14509	0.07290	0.05106	0.01394

Table 2. Rate of heat transfer at the plate $(\eta=0)$ and at the plate $(\eta=1)$

	$-\theta'(0)$				$-\theta'(1)$			
$R\backslash\tau$	0.1	0.2	0.3	0.4	0.1	0.2	0.3	0.4
0.5	0.12551	0.24165	0.35779	0.47392	0.08767	0.17980	0.27193	0.36405
1.0	0.14014	0.27144	0.40275	0.53405	0.08110	0.16619	0.25128	0.33637
1.5	0.15398	0.29960	0.44522	0.59084	0.07518	0.15396	0.23273	0.31151
2.0	0.16712	0.32631	0.48550	0.64469	0.06984	0.14292	0.21601	0.28909

CONCLUSION

The radiation effects on MHD free convective flow in a rotating system confined between two infinitely long vertical walls with variable temperature have been studied. The magnetic field has an accelerating influence on both the primary and the secondary velocity. The effect of the rotation is very important in the velocity field. In the prence of radiation the primary velocity reduces whereas the secondary velocity accelerates. An increase in either radiation parameter R or Prandtl number Pr leads to fall in the fluid temperature θ. There is an enhancement in fluid temperature as time progresses. Both the rotation and radiation enhance the absolute value of the shear stress τ_{x_0} at the wall $(\eta=0)$ and reduce the absolute value of the shear stress τ_{y_0} at the wall $(\eta=0)$. Further, the rate of heat transfer $-\theta'(0)$ at the wall $(\eta=0)$ increases whereas the rate of heat transfer $-\theta'(1)$ at the wall $(\eta=1)$ decreases with an increase in radiation parameter R.

REFERENCES

[1] A.K. Singh, *Defense Science Journal*, **1988**, 38(1), 35-41.
[2] A.K. Singh, T. Paul, *Int. J. Appl. Mech. Eng.*, **2006**, 11(1), 143-154.
[3] B.K. Jha, A.K. Singh, H.S. Takhar, *Int. J. Appl. Mech. Eng.*, **2003**, 8(3), 497-502.
[4] H.M. Joshi, *Int. Comm. in Heat and Mass Transfer*, **1988**, 15, 227-238.

[5] O. Miyatake and T. Fujii, *Heat Transfer Japan Res.*, **1972**, 1, 30-38.
[6] H.Tanaka, O. Miyatake, T. Fujii, M. Fujii, *Heat Transfer Japan Res.*, **1973**, 2, 25-33.
[7] A.R. Bestman, S.N. Adjepong, *Space Sci*., **1988**, 143, 73-80.
[8] A.K. Singh, H.R. Gholami and V.M. Soundalgekar, *Heat and Mass Transfer*, **1996**, 31, 329-331.
[9] B.K. Jha, *Heat and Mass Transfer*, **2001**, 37, 329-331.
[10] M. Narahari, S. Sreenadh, V.M. Soundalgekar, *J. Thermophysics and Aeromechanics*, **2002**, 9(2), 287-293.
[11] P. Mebine, J. Global, *Pure and Appl. Math.*, **2007**, 3(2), 1-12.
[12] B.K. Jha, A.O. Ajibade, *Int. J. Energy and Tech.*, **2010**, 2(12), 1–9.
[13] M. Narahari, *WSEAS Transactions on Heat and Mass Transfer*, **2010**, 5(1), 21-30.
[14] A.G.V. Kumar, S.V.K Varma, *Int. J. Eng. Sci. Tech.*, **2011**, 3(4), 2897-2909.
[15] U.S. Rajput, P.K. Sahu, *Int. J. Math. Analysis*, **2011**, 5(34), 1665-6671.
[16] U.S. Rajput, S. Kumar, *Int. J. Math. Analysis*, **2011**, 5(24), 1155 - 1163.
[17] S. S. Saxena, G.K. Dubey, *Adva. Appl. Sci. Res*., **2011**, 2 (4), 259-278.
[18] V. Sri Hari Babu, G.V. Ramana Reddy, *Adva. Appl. Sci. Res*., **2011**, 2 (4), 138-146.
[19] S. S. Saxena, G.K. Dubey, *Adva. Appl. Sci. Res*., **2011**, 2 (5), 115-129.
[20] G. Sudershan Reddy, G.V. Ramana Reddy, K. Jayarami Reddy, *Adva. Appl. Sci. Res*., **2012**, 3(3), 1603-1610.
[21] S.P. Anjali Devi, A. David Maxim Gururaj, *Adva. Appl. Sci. Res*., **2012**, 3 (1), 319 - 334.
[22] K. Jayarami Reddy, K. Sunitha, M. Jayabharath Reddy, *Adva. Appl. Sci. Res*., **2012**, 3(3), 1231-1238.
[23] S. Das, B.C. Sarkar, R.N. Jana , *Open J. Fluid Dynamics*, **2012**, 2, 14-27.
[24] C. Mandal, S. Das, R.N. Jana, *Int. J. Appl. Inf. Systems*, **2012**, 2(2), 49-56.
[25] S. Das, S.K. Guchhait, R.N. Jana, *Int. J. Com. Appl.*, **2012**, 39(3), 42-51.
[26] B.C. Sarkar, S. Das S, R.N. Jana, *Int. J. Eng. Res. and Appl.*, **2012**, 2(4), 2346-2359.
[27] A.C. Cogley, W.C. Vincentine, S.E. Gilles, *Am. Inst. Aeronat. Astronaut. J.*, **1968**, 6, 551-555.